Available online at www.sciencedirect.com
SCIENCE DIRECT®
International Journal of Heat and Mass Transfer 48 (2005) 4150–4160
International Journal of HEAT and MASS TRANSFER
www.elsevier.com/locate/ijhmt

Mixed convection from two thermal sources in a vertical porous layer

Nawaf H. Saeid [a,*], Ioan Pop [b]

[a] School of Mechanical Engineering, University of Science Malaysia, 14300 Nibong Tebal, Pulau Pinang, Malaysia
[b] Faculty of Mathematics, University of Cluj, R-3400 Cluj, CP 253, Romania

Received 7 October 2004; received in revised form 13 February 2005

Abstract

In this paper the steady mixed convection flow adjacent to a vertical surface embedded in a fluid-saturated porous medium, on which two isolated thermal sources are located is investigated theoretically. The thermal sources are taken as long planar sources of finite height and the resulting two-dimensional flow is numerically studied using the finite volume method. The nature and the basic characteristics of the mixed aiding as well as mixed opposing flows that arise are investigated using the Darcy law model. The governing parameters are the Rayleigh number, Péclet number, separation distance between heated elements, their lengths and heat flux ratio in additional to the external flow direction. These parameters are varied over wide ranges and their effect on the heat transfer characteristics is studied in detail.

1. Introduction

Over the past years considerable research efforts have been devoted to the study of heat transfer induced by buoyancy effects in a porous medium saturated with fluids. Interest in this convective flow phenomenon has been motivated by such diverse engineering problems as geothermal energy extraction, underground heat exchangers for energy storage, recovery and temperature-controlled reactors, electronic systems cooling, petroleum reservoirs, groundwater hydrology, coal combustors, grain storage, fiber and granular insulation, to name just a few applications of the topic of convective flow in porous media. Several monographs and recent review articles summarizing the state-of-the-art available in the literature testify to the maturity of this area; see for example, [1–9].

The existing literature on this domain has focused considerable attention on natural and mixed convection in two-dimensional horizontal or vertical porous layers. Lai et al. [10–12], and Prasad et al. [13], have studied numerically the steady free and mixed convection in a porous channels with a finite, isothermal heat sources centrally located on one horizontal or vertical wall. Lai and Kulacki [14] reported experimental results for free and mixed convection in liquid saturated, horizontal porous layers with localized heating from below. Based on dimensional analysis and non-linear regression, correlations for the average Nusselt number against Rayleigh and Peclet numbers have been obtained. It is shown that the values of the average Nusselt number compare very well with the numerically calculated

* Corresponding author. Present address: Department of Mechanical Engineering, Curtin University of Technology, CDT 250, 98009 Miri, Sarawak, Malaysia. Tel.: +60 85 443 964; fax: +60 85 443 838.
E-mail address: n_h_saeid@yahoo.com (N.H. Saeid).

0017-9310/$ - see front matter © 2005 Elsevier Ltd. All rights reserved.
doi:10.1016/j.ijheatmasstransfer.2005.04.023

Nomenclature

d	separation distance between heated elements, Fig. 1
g	gravitational acceleration
K	permeability of the porous medium
k_m	effective thermal conductivity of the porous medium
l_1, l_2	lower and upper heat source length, respectively, Fig. 1
Nu_1, Nu_2	local Nusselt number for the lower and upper heat source respectively
$\overline{Nu_1}, \overline{Nu_2}$	average Nusselt number along the lower and upper heat source respectively
Pe	Péclet number, $Pe = V_\infty l_1/\alpha_m$
q_1, q_2	constant heat flux for lower and upper heat source, respectively, Fig. 1
Ra	Rayleigh number for porous medium, $Ra = g\beta K(q_1 l_1/k_m)l_1/v\alpha_m$
s_1, s_2	distances from the lower and upper sides of the heat source respectively, Fig. 1
T	fluid temperature
T_∞	ambient temperature
u, v	velocity components along x- and y-axes, respectively
V_∞	free stream velocity
U, V	non-dimensional velocity components along X- and Y-axes, respectively
x, y	Cartesian coordinates
X, Y	non-dimensional Cartesian coordinates

Greek symbols

α_m	effective thermal diffusivity
β	coefficient of thermal expansion
θ	non-dimensional temperature
v	kinematic viscosity
Ψ	non-dimensional stream function

values. However, an excellent review paper on this topic has been presented by Lai [15], and the references mentioned therein.

The present paper deals with a numerical study of the mixed convection flow caused by an aligned stream of fluid flowing past a vertical surface embedded in a fluid-saturated porous medium on which two long isolated thermal sources, of finite height and dissipating a uniform heat flux are located. Both aiding and opposing natural and forced convection mechanisms are considered. The same problem was considered for a viscous and incompressible fluid (non-porous media) by Jaluria [16] but only for aiding mixed convection flow. Though the preceding studies focus on two-dimensional convection flow in porous layers or cavities with one, two or multiple discrete heating, the external flow configuration received little attention although problems of this type are frequently encountered in the applications.

2. Governing equations

A schematic diagram of a two-dimensional mixed convection flow from two isoflux heat sources located in a vertical porous layer of ambient temperature T_∞ is shown in Fig. 1, along with the coordinate system employed. Two heat sources of heights l_1 and l_2 are located on a vertical adiabatic surface and separated by a distance d, the plate being embedded in a fluid-saturated porous medium. The transverse dimension is assumed to be large so that the flow may be approximated as two-dimensional. The free-stream velocity V_∞ is taken as vertically upward for the aiding flow considered (Fig. 1(a)) and vertically downward for the opposing flow considered (Fig. 1(b)), respectively. The thermal sources are assumed to impart a uniform heat flux input into the flow, these inputs being denoted by q_1 and q_2, respectively. In the porous medium, Darcy's law is assumed to hold, and the fluid is assumed to be a normal Boussinesq fluid. The viscous drag and inertia terms in the governing equations are neglected, which are valid assumptions for low Darcy and particle Reynolds numbers.

To ensure the accuracy of the results, the full two-dimensional equations are considered instead of the boundary layer equations. Therefore, the continuity, Darcy and energy equations for steady flow in an isotropic and homogeneous porous medium can be written as

$$\frac{\partial u}{\partial x} + \frac{\partial v}{\partial y} = 0 \tag{1}$$

$$\frac{\partial u}{\partial y} - \frac{\partial v}{\partial x} = -\frac{g\beta K}{v}\frac{\partial T}{\partial y} \tag{2}$$

$$u\frac{\partial T}{\partial x} + v\frac{\partial T}{\partial y} = \alpha_m\left(\frac{\partial^2 T}{\partial x^2} + \frac{\partial^2 T}{\partial y^2}\right) \tag{3}$$

where u, v are the Darcy's velocity components along x- and y-axes, T is the fluid temperature, and the physical meaning of the other quantities are mentioned in the Nomenclature. The governing equations (1)–(3) can be written in non-dimensional form by using the following non-dimensional variables:

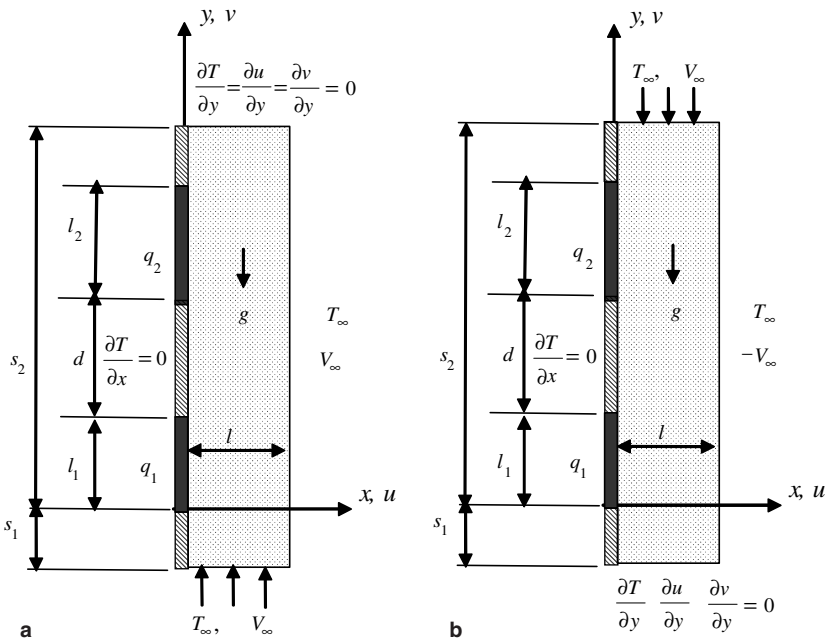

Fig. 1. Schematic diagram of the physical model and the coordinate system: (a) aiding flow; (b) opposing flow.

$$U=\frac{u}{V_\infty}=\frac{\partial \Psi}{\partial Y};\quad V=\frac{v}{V_\infty}=-\frac{\partial \Psi}{\partial X};\quad \theta=\frac{T-T_\infty}{q_1 l_1/k_m} \tag{4}$$

together with non-dimensionalisation of all the lengths based on the length of the lower heat source (l_1) and denoting them by respective capital letters, leads to the following dimensionless forms of the governing equations:

$$\frac{\partial^2 \Psi}{\partial X^2}+\frac{\partial^2 \Psi}{\partial Y^2}=-\frac{Ra}{Pe}\frac{\partial \theta}{\partial X} \tag{5}$$

$$\frac{\partial \Psi}{\partial Y}\frac{\partial \theta}{\partial X}-\frac{\partial \Psi}{\partial X}\frac{\partial \theta}{\partial Y}=\frac{1}{Pe}\left(\frac{\partial^2 \theta}{\partial X^2}+\frac{\partial^2 \theta}{\partial Y^2}\right) \tag{6}$$

where Ra is the Rayleigh number for porous medium defined as $Ra = g\beta K(q_1 l_1/k_m)l_1/\nu\alpha_m$, Pe is the Péclet number defined as $Pe = V_\infty l_1/\alpha_m$. The dimensionless boundary conditions are

$$\Psi(0,Y)=0;$$

$$\frac{\partial \theta(0,Y)}{\partial X}=-1 \quad \text{for } 0\leqslant Y\leqslant 1;$$

$$\frac{\partial \theta(0,Y)}{\partial X}=-\frac{q_2}{q_1} \quad \text{for } (1+D)\leqslant Y\leqslant (1+D+L_2)$$

$$\text{and otherwise adiabatic } \frac{\partial \theta(0,Y)}{\partial X}=0 \tag{7a}$$

$$\Psi(L,Y)=-1 \quad \text{for aiding flow, and}$$
$$\Psi(L,Y)=1 \quad \text{for opposing flow;}\quad \theta(L,Y)=0 \tag{7b}$$

$$\Psi(X,-S_1)=-X,\quad \theta(X,-S_1)=0 \quad \text{for aiding flow}$$

$$\frac{\partial \Psi(X,-S_1)}{\partial Y}=\frac{\partial \theta(X,-S_1)}{\partial Y}=0 \quad \text{for opposing flow} \tag{7c}$$

$$\frac{\partial \Psi(X,S_2)}{\partial Y}=\frac{\partial \theta(X,S_2)}{\partial Y}=0 \quad \text{for aiding flow}$$

$$\Psi(X,S_2)=X,\quad \theta(X,S_2)=0 \quad \text{for opposing flow} \tag{7d}$$

It can be seen from the above formulation that the governing parameters are Ra, Pe, D, L_2 and q_2/q_1. The physical quantities of particular interest in this problem are the local Nusselt numbers along the heat sources, defined as

$$Nu_1=\frac{q_1 l_1}{k_m(T_w-T_\infty)}=\frac{1}{\theta_w} \tag{8a}$$

$$Nu_2=\frac{q_2 l_2}{k_m(T_w-T_\infty)}=\frac{L_2(q_2/q_1)}{\theta_w} \tag{8b}$$

and also the average Nusselt numbers along the heat sources, which are calculated as

$$\overline{Nu_1}=\int_0^1 Nu_1\,dY;\quad \overline{Nu_2}=\frac{1}{L_2}\int_{1+D}^{1+D+L_2} Nu_2\,dY \tag{9}$$

3. Numerical method

Eqs. (5) and (6) subjected to the boundary conditions (7) are integrated numerically using the finite volume method, which is described in the book by Patankar [17]. The central differencing scheme is used for the diffusion terms of the energy equation (6) as well as for the momentum equation (5). The quadratic upwind differencing QUICK scheme given by Hayase et al. [18] is used for the convection terms formulation of the energy equation (6). This scheme has a third-order accurate approximation for the uniform grid spacing. The linear extrapolation, known as mirror node approach, has been used for the boundary conditions implementation. The resulting algebraic equations were solved by line-by-line iteration using the tri-diagonal matrix algorithm. The iteration process is terminated under the following condition:

$$\sum_{i,j} |\phi^{n}_{i,j} - \phi^{n-1}_{i,j}| \Big/ \sum_{i,j} |\phi^{n}_{i,j}| \leqslant 10^{-5} \tag{10}$$

where ϕ is the general dependent variable which can stands for either θ or Ψ and n denotes the iteration step. In the present study, it is assumed that the width of the solution domain is equal to the heat source length, or $L = 1$. The lengths on the upstream and down stream sides of the heat sources (S_1 and S_2) have been changed as function of flow direction, the upper heat source length L_2 and the separation distance D in order to ensure the correct boundary conditions (7c) and (7d).

The developed code is essentially a modified version of a code built and validated for mixed convection flow along isothermal heat source in a recent paper by Saeid [19]. Moreover, the results of the present numerical scheme for the case of single constant heat flux source ($L_2 = 0$) are compared with the results obtained by Cheng [20] and Hsieh et al. [21] based on the boundary layer flow. The present study is limited for the mixed convection mode with Rayleigh number range $10 \leqslant Ra \leqslant 100$, in which Darcy model is applicable and Péclet number range $0.1 \leqslant Pe \leqslant 100$. It is important to note that the boundary layer flow can be approximated for high values of the Péclet number only, see Fig. 4 (note that only the important region is shown in the contour plots). Therefore, the results of the present study are compared with the results obtained by Cheng [20] and Hsieh et al. [21], based on the boundary layer assumptions, for $Pe = 100$.

For pure forced convection ($Ra = 0$ and high Pe), Cheng [20] found the local Nusselt number $Nu = 0.886\sqrt{Pe}$ and the average Nusselt number, $\overline{Nu} = 1.329\sqrt{Pe}$. For the same pure forced convection Hsieh et al. [21] obtained the local Nusselt number $Nu = 0.8863\sqrt{Pe}$, which is in good agreement with Cheng's [20] result, but the correlation given by Hsieh et al. [21] for the average Nusselt number gives $\overline{Nu} = 1.7727\sqrt{Pe}$ with a difference of 33% higher than the value obtained by Cheng [20]. The results of the present study, with $Pe = 100$ and $Ra = 0$, are $Nu/\sqrt{Pe} = 0.8866$, which is calculated at the upper end of the heat source, and $\overline{Nu}/\sqrt{Pe} = 1.6240$, respectively. The present result of the local Nusselt number is in good agreement with the results of Cheng [20] for forced convection and Hsieh et al. [21] for mixed convection as shown in Table 1. The average Nusselt number values show difference from that obtained from the correlation given by Hsieh et al. [21] as shown in Table 1 but the present value for forced convection ($Ra = 0$) is in between the values of Cheng [20] and Hsieh et al. [21]. It important to mention that Hsieh et al. [21] have indicated that their correlation for average Nusselt number has a maximum deviation of about 5% from their results obtained using the boundary layer theory over the entire regime of mixed convection. Moreover the steep variation of the temperature near the leading edge of the heat source has an important effect on the accuracy of the average Nusselt number along the heat source. It is evident that the leading edge effect leads to inaccurate results using the boundary layer approximation compared with the results obtained from solving the full set of governing equations.

Table 1
Values of the local and average Nusselt numbers of the single heat source in mixed convection mode, with $Pe = 100$ and different values of Ra

Ra	$Nu(Pe^{1/2} + Ra^{1/3})^{-1}$		$\overline{Nu}(Pe^{1/2} + Ra^{1/3})^{-1}$	
	Hsieh et al. [21]	Present	Hsieh et al. [21]	Present
0	0.8863	0.8866	1.7727	1.6240
10	0.7310	0.7313	1.4598	1.3386
20	0.7002	0.7009	1.3968	1.2820
40	0.6663	0.6674	1.3259	1.2190
60	0.6453	0.6469	1.2810	1.1800
80	0.6302	0.6321	1.2480	1.1513
100	0.6185	0.6207	1.2219	1.1280

The grid independence test is performed for equal spacing mesh with two different sizes (100×300) and (200×600) for the domain defined by $S_1 = 3$ and $S_2 = 7$ for the aiding mixed convection of a single heat source. The results show that the difference is about 1% in the calculation of $\overline{Nu}(Pe^{1/2} + Ra^{1/3})^{-1}$ using the above two mesh sizes. Larger values of S_1 and/or S_2 have no significant effect on the results, which reflect the accuracy of implementing the boundary conditions (7).

For mixed convection from two heat sources the solution domain is doubled ($S_1 + S_2 = 20$) for all the flow conditions considered later and $S_1 = 3$ is fixed for all the aiding flow cases, while it is changed for opposing flow conditions to ensure independence of the results.

For example the test consider for opposing flow over two heat sources with the maximum Ra, Pe and separation distance considered in the present study ($D = 8$ with $Ra = 100$ and $Pe = 100$), it is found that $S_1 = 7$ is sufficiently large to ensure accurate results. The mesh size is doubled also in the Y direction but it is same in the X direction as the single heat source, i.e., (100×600). The grid independence test and size of the solution domain are performed also for both aiding and opposing mixed convection from two heat sources for the maximum Ra, Pe and separation distance considered in the present study ($D = 8$ with $Ra = 100$ and $Pe = 100$). The results obtained using (100×600) and (200×1200) nodes are compared and it is found that the difference is less than 1% for average Nusselt number along the lower heat source while it is less than 0.2% along the upper heat source in the aiding flow. The results for opposing flow using the above mesh sizes show a difference of 0.25% for average Nusselt number along the upper heat source and 1.2% along the lower heat source.

Again these comparisons support very well the validity of the present computations. It is important to note that the number of iteration steps required satisfying the convergence condition (10) is increasing with increasing the mesh size and this practice is always a balance of convergence and computational time. Therefore the solution domain is fixed ($S_1 + S_2 = 20$) for all the flow conditions and the mesh size (100×600) is used to generate the results.

4. Results and discussion

The results are generated to show the effect of the governing parameters D, L_2, q_2/q_1, Pe and Ra in additional to the external flow direction on the average Nusselt number along both the heated elements shown in Fig. 1.

4.1. Effect of the separation distance

The variation of average Nusselt number, $\overline{Nu}$, with Péclet number, Pe, at various values of the separation distance, D, is shown in Fig. 2 with $Ra = 10$, $L_2 = 1$ and $q_2/q_1 = 1$. It is seen that the effect of the Péclet number and the flow direction are not distinguishable for buoyancy dominated driven flows (low Pe) and the average Nusselt number along the two heat sources is approximately constant, as shown in Fig. 2. However, for an aiding flow and higher values of Pe, Fig. 2 shows that $\overline{Nu_1}$ increases with the increase of Pe and the variation of $\overline{Nu_1}$ with different values of D, forms a single curve. This demonstrates that the heat transfer from the lower heat source is not affected by the presence of the upper heat source with different separation distances since the buoyancy flow, as well as, the external flow

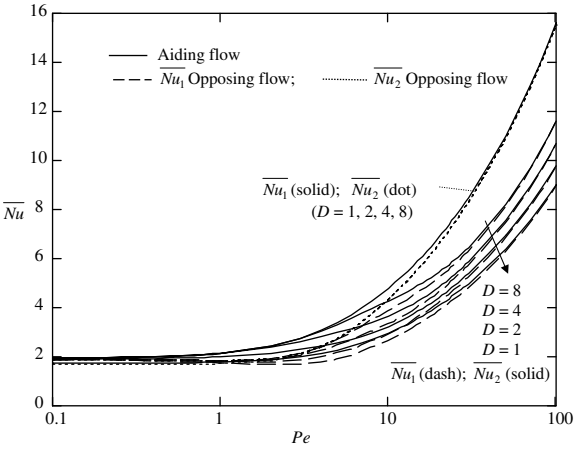

Fig. 2. Variation of the average Nusselt number with Péclet number at various values of the separation distance with $Ra = 10$, $L_2 = 1$ and $q_2/q_1 = 1$.

derives upwards. For the same case of aiding flow, the values of $\overline{Nu_2}$ are increasing with increasing either Pe or the separation distance D. For high values of D and low Pe the heat transfer from the two sources are approximately equal since the flow is buoyancy driven and the separation distance is large enough, as shown in Fig. 2, see for example $\overline{Nu_1} \cong \overline{Nu_2}$ at $D = 8$ and $Pe < 5$. Further, with $Ra = 10$ and low values of Péclet number ($Pe < 2$), as well as high values of Péclet number ($Pe > 40$), Fig. 2 shows there is a difference between the values of the average Nusselt number when the aiding and opposing flows are small. The values of $\overline{Nu_2}$ are forming a single curve in the opposing flow, where the external flow passes through the upper heat source first. Fig. 2 also shows that, for $Pe > 2$, the values of average Nusselt number along the both sources increases with the increase of the Péclet number for both aiding and opposing flows, respectively. The values of $\overline{Nu_1}$ are increasing with increasing either Pe or the separation distance D, as can be seen from Fig. 2. The effect of the separation distance, D, on the variation of average Nusselt number with Péclet number is shown in Fig. 3 for higher values of the Rayleigh number ($Ra = 100$) and same selected values of $L_2 = 1$ and $q_2/q_1 = 1$. For aiding flows and $Ra = 100$ similar observations as those mentioned for $Ra = 10$ can be pointed out from Fig. 3. The thermal and flow fields for aiding flow with $Ra = 100$, $D = 2$, $L_2 = 1$, $q_2/q_1 = 1$ and different values of Pe are illustrated in Fig. 4. At $Pe = 1$, two clockwise rotation cells are observed near the two thermal sources, which indicate the buoyancy domination heat transfer, as shown in Fig. 4(a). As the external flow increases, Fig. 4(b) and (c) show that a boundary layer is developed and the isotherms and the streamlines indicate the forced convection domination at $Pe = 100$.

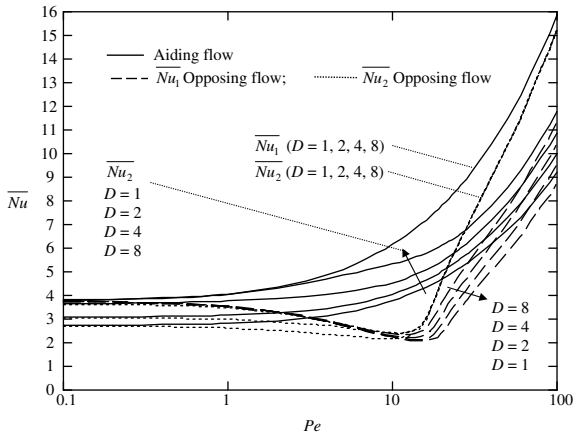

Fig. 3. Variation of the average Nusselt number with Péclet number at various values of the separation distance with $Ra = 100$, $L_2 = 1$ and q_2/q_1.

For opposing flows, on the other hand, with $Ra = 100$, the variation of average Nusselt number against the Péclet number shows different features than those with $Ra = 10$. Thus, at relatively small values of Pe, the values of the average Nusselt number along both sources are decreasing with increasing Pe. The isotherms and stream lines for $Pe = 10$ with $Ra = 100$, $D = 2$, $L_2 = 1$ and $q_2/q_1 = 1$ depicted in Figs. 4(a) and 5(a) are almost similar for both aiding and opposing flows, respectively. Both $\overline{Nu_1}$ and $\overline{Nu_2}$ reach a minimum value in the range $10 < Pe < 20$, where a balance between the buoyancy and external flows is expected. The values of $\overline{Nu_1}$ in the opposing flow case with $Ra = 100$ and some moderate values of Pe are less than those with $Ra = 10$ presented in Fig. 2. When the values of $\overline{Nu}$ are minimum, there will be approximately a stagnant region near the heat sources as shows Fig. 5(b) for $Pe = 10$ with $Ra = 100$, $D = 2$, $L_2 = 1$ and $q_2/q_1 = 1$. Increasing Pe further beyond the value which gives minimum Nusselt

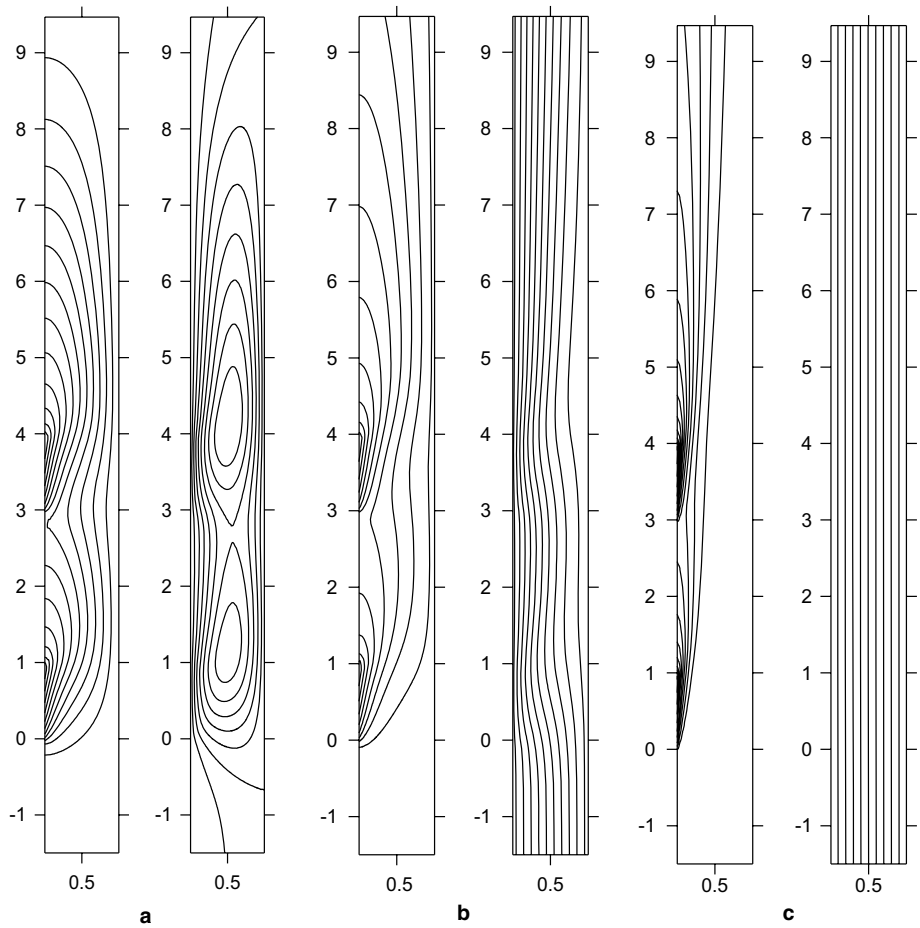

Fig. 4. Isotherms (left) and stream lines (right) for aiding flow, $Ra = 100$, $D = 2$, $L_2 = 1$ and $q_2/q_1 = 1$. (a) $Pe = 1$ ($\Delta\theta = 0.03$, $\Delta\Psi = 0.5$), (b) $Pe = 10$ ($\Delta\theta = 0.03$, $\Delta\Psi = 0.1$) and (c) $Pe = 100$ ($\Delta\theta = 0.01$, $\Delta\Psi = 0.1$) (note that only the important region is shown in the contour plots).

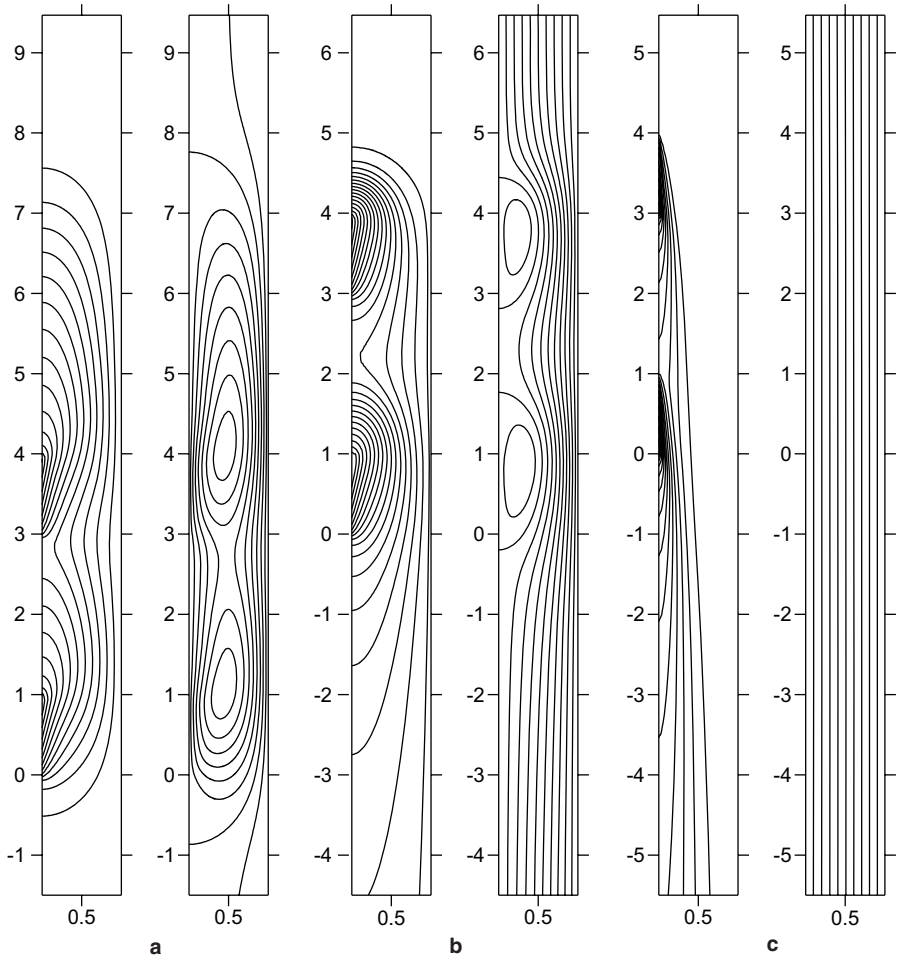

Fig. 5. Isotherms (left) and stream lines (right) for opposing flow, $Ra = 100$, $D = 2$, $L_2 = 1$ and $q_2/q_1 = 1$. (a) $Pe = 1$ ($\Delta\theta = 0.03$, $\Delta\Psi = 0.5$), (b) $Pe = 10$ ($\Delta\theta = 0.03$, $\Delta\Psi = 0.1$) and (c) $Pe = 100$ ($\Delta\theta = 0.01$, $\Delta\Psi = 0.1$).

number leads to enhance the heat transfer, where the external flow is gradually dominated, see Fig. 3. Further, Fig. 3 shows for opposing flows with $Pe > 20$ that, increasing either Pe or the separation distance D will increase the values of $\overline{Nu_1}$. At high values of Pe the values of $\overline{Nu_1}$ for opposing flows with different separation distances approach the corresponding values of $\overline{Nu_2}$ for aiding flows with respective separation distances. It can be also seen from Fig. 3 that increasing $Pe > 20$, the values of $\overline{Nu_2}$ are forming a single curve with different values of D for opposing flows. This indicates the domination of the external downward flow and the presence of the lower source does not affect the heat transfer from the upper source. Figs. 4(c) and 5(c) show that the flow and thermal fields are almost identical for aiding and opposing flows, respectively, but in the opposite direction. Therefore, the values of $\overline{Nu_2}$ for opposing flows approach the corresponding values of $\overline{Nu_1}$ for aiding flows at high values of Pe, as shown in Fig. 3. Comparing the result presented in Figs. 2 and 3 reveals that the Rayleigh number has more effect when Pe is small (buoyancy driven flow) than that at high values of Pe (external driven flows) for all the separation distances D.

4.2. Effect of the length ratio of the heat sources

The effect of the length L_2 of the upper heat source normalized by the length of the lower heat source on the mixed convection flow is discussed now for both aiding and opposing external flows with fixed values of $Ra = 100$, $D = 2$ and $q_2/q_1 = 1$. For aiding flows, Fig. 6 shows that $\overline{Nu_1}$ is increasing with increasing Pe and his values are forming a single curve for different values of L_2, while the values of $\overline{Nu_2}$ are increasing with increasing L_2. However, the values of $\overline{Nu_2}$ are higher than those of $\overline{Nu_1}$ at high values of L_2. The increase in $\overline{Nu_2}$ is basically due to the increase of the effective Rayleigh number (Ra_2) for the upper heat source, where it can be shown

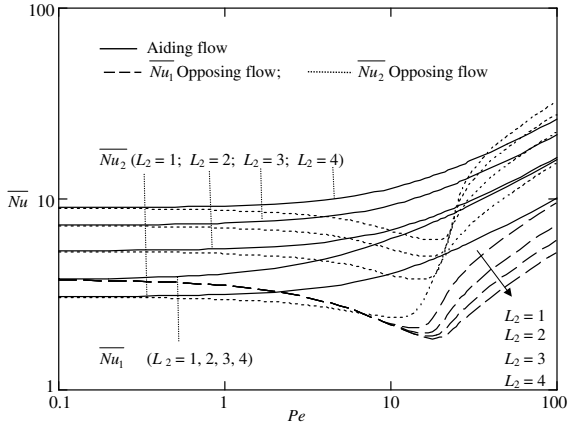

Fig. 6. Variation of the average Nusselt number with Péclet number various values of the upper source length with $Ra = 100$, $D = 2$ and $q_2/q_1 = 1$.

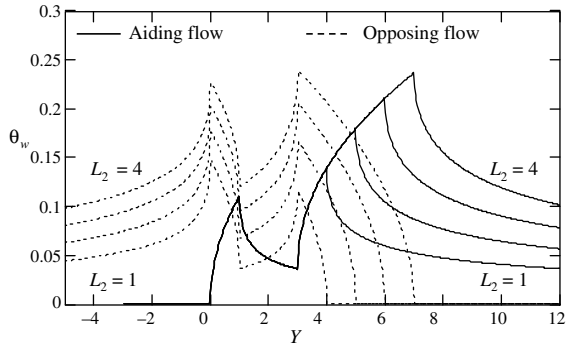

Fig. 7. Surface temperature along the vertical wall at various values of the upper source length ($L_2 = 1$, 2, 3 and 4) with $Ra = 100$, $Pe = 100$, $D = 2$ and $q_2/q_1 = 1$.

that $Ra_2 = Ra \times (q_2/q_1) \times (L_2)^2$. Fig. 7 shows the variation of the surface temperature along the whole vertical wall at various values of the upper source lengths with $Ra = 100$, $Pe = 100$, $D = 2$ and $q_2/q_1 = 1$. It can be seen that for aiding flow the surface temperature along the lower heat source is increasing and it drops sharply in the adiabatic region between the two sources. This temperature distribution is not affected by the presence of the upper heat source, and therefore, the values of $\overline{Nu_1}$ are forming a single curve, as mentioned earlier. For the same aiding flow, Fig. 7 shows that the surface temperature along the upper heat source is increasing and it is decreasing sharply in the adiabatic regions above the heat source. However, the maximum surface temperature at the upper end of the upper heat source is higher than that of the lower heat source but still $\overline{Nu_2}$ is higher than $\overline{Nu_1}$ for high values of L_2 due to high values of effective Rayleigh number.

For low values of Pe and opposing flow case, Fig. 6 shows that $\overline{Nu_1}$ is decreasing with increasing Pe and it reaches a minimum value at around $Pe = 20$ for all the values of L_2. The values of $\overline{Nu_1}$ calculated with different values of L_2 are forming a single curve only for $Pe < 10$ where buoyancy flow is dominant and the presence of the upper heat source is not important. For $Pe > 10$, on the other hand, the effect of the upper heat source on $\overline{Nu_1}$ is much more distinct. Here the external opposing flow starts to affect the flow along the lower heat source, which is located in the wake of the upper heat source. It is found that $\overline{Nu_1}$ is decreasing with increasing the upper heat source length, as shown in Fig. 6, because longer upper heat source generates higher fluid temperatures near the lower heat source in the high Pe opposing flow case, as can be seen in Fig. 7. For low Pe opposing flow case, the values of $\overline{Nu_2}$ are decreasing with either increasing Pe or decreasing L_2 for the buoyancy driven flows (low Pe), as shown in Fig. 6. The values of $\overline{Nu_2}$ for different upper heat source lengths reach the minimum value about in the range $20 \leqslant Pe \leqslant 30$ for all values of L_2, where a balance between the buoyancy and external flows is expected. Further increase in Pe, the values of $\overline{Nu_2}$ curves start increasing with Pe and higher heat source lengths results in higher values of $\overline{Nu_2}$. For high Pe opposing flows, Fig. 6 shows that the values of $\overline{Nu_2}$ with $L_2 = 2$, 3 and 4 are higher than the corresponding values for the aiding flow case. This indicates the external flow domination and there is a fresh fluid flow around the upper heat source instead of the heated fluid in the aiding flow case. Fig. 7 also shows that the maximum surface temperature of the upper heat source for opposing flows is less than that for aiding flows for a given value of L_2.

4.3. Effect of the heat flux ratio

Finally, the effect of the heat flax ratio on the mixed convection is studied for both aiding and opposing external flows with fixed values of $Ra = 100$, $D = 2$ and $L_2 = 1$. For aiding flows, Fig. 8 shows that both $\overline{Nu_1}$ and $\overline{Nu_2}$ are increasing with increasing Pe and the values of $\overline{Nu_1}$ with different values of q_2/q_1 are forming a single curve indicating that the heat transfer from the lower heat source is independent on the presence of the upper element with the given parameters. On the other hand, the values of $\overline{Nu_2}$ are increasing with increasing q_2/q_1 and these values are higher than those of $\overline{Nu_1}$ at high values of q_2/q_1 and low Pe. The increase in $\overline{Nu_2}$ is again due to the increase of the effective Rayleigh number for the upper heat source, where it can be shown that Ra_2 is given by $Ra_2 = Ra \times (q_2/q_1) \times (L_2)^2$. It has been previously shown in Figs. 2 and 3 that the effect of the Rayleigh number is diminished as Péclet number increases. Therefore, Fig. 8 shows that at high values of Pe the values of $\overline{Nu_1}$ are higher than those of $\overline{Nu_2}$ for given values of q_2/q_1.

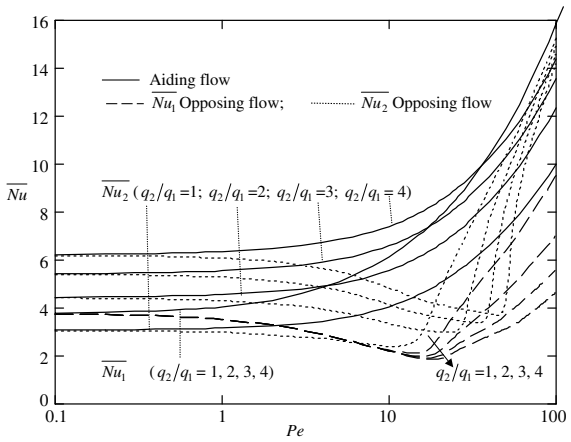

Fig. 8. Variation of the average Nusselt number with Péclet number at various values of the heat flux ratio q_2/q_1 with $Ra = 100$, $D = 2$ and $L_2 = 1$.

In the opposing flow cases, for small values of Péclet number ($Pe < 10$) and all the heat flux ratios, Fig. 8 shows that the average Nusselt number along both the heat sources are decreasing with increasing Pe due to the slow down flow along the heat sources caused by the interaction between the buoyancy and the external flows. Fig. 8 also shows that the values of $\overline{Nu_1}$ and $\overline{Nu_2}$ reach a minimum value at different values of Péclet number depending on the heat flux ratio. However, for large values of Péclet number, the average Nusselt number along both the heat sources are increasing with increasing Pe due to the domination of the forced convection mode. The value of Péclet number, at which the forced convection is dominant, depends on the heat flux ratio. It is evident that the buoyancy forces along the upper source are increasing with increasing the heat flux from the upper source. This leads the necessity of high value of Péclet number in order to overcome the buoyancy flow for high values of heat flux ratios, as Fig. 8 shows.

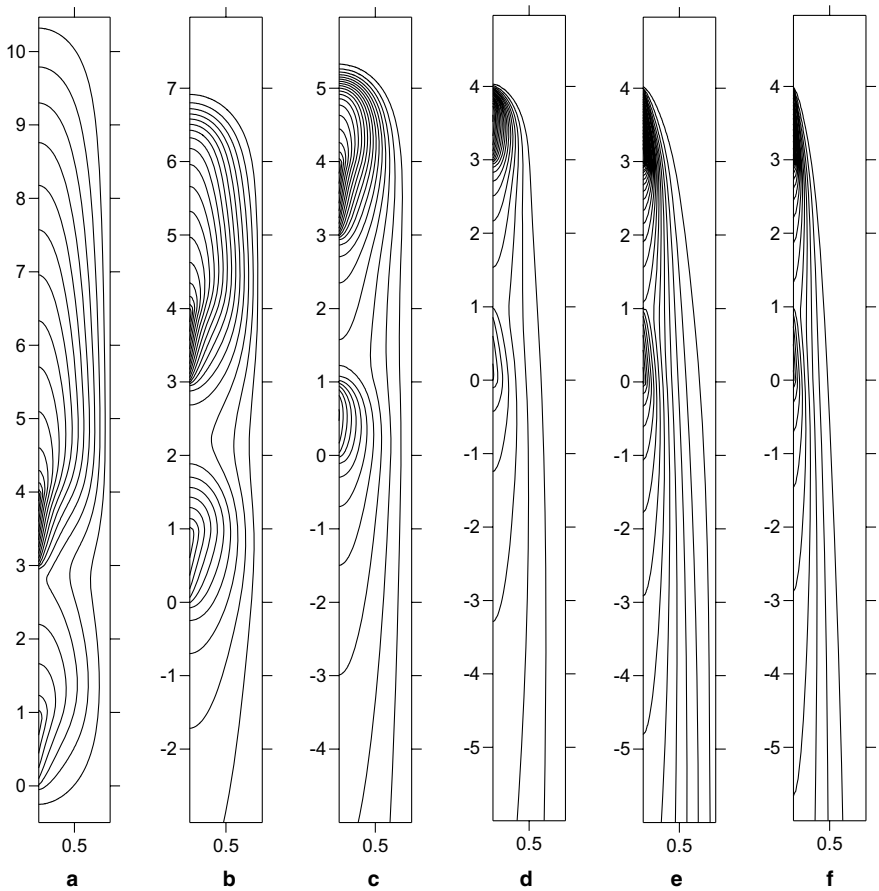

Fig. 9. Isotherms for opposing flow, $Ra = 100$, $D = 2$, $L_2 = 1$ and $q_2/q_1 = 3$. (a) $Pe = 1$ ($\Delta\theta = 0.05$), (b) $Pe = 10$ ($\Delta\theta = 0.05$), (c) $Pe = 20$ ($\Delta\theta = 0.05$), (d) $Pe = 40$ ($\Delta\theta = 0.05$), (e) $Pe = 60$ ($\Delta\theta = 0.02$) and (f) $Pe = 100$ ($\Delta\theta = 0.02$).

The interesting results illustrated in Fig. 8 are the effect of increasing the heat flux ratio with moderate values of Péclet number. When the heat flux ratio is high, for example, $q_2/q_1 = 3$, and Pe between 20 and 40, it can be seen that $\overline{Nu_1}$ is increasing with increasing Pe, in contrast to that, $\overline{Nu_2}$ is decreasing with increasing Pe. $\overline{Nu_2}$ is decreasing because at high q_2/q_1 the buoyancy forces are strong enough to oppose the external flow near the upper source. In contrast to that, $\overline{Nu_1}$ is increasing because the external flow is strong enough to oppose the buoyancy flow generated near the lower source, which is in this case three times less than that at the upper heat source.

The details of the thermal field for opposing flow case with $Ra = 100$, $D = 2$, $L_2 = 1$ and $q_2/q_1 = 3$ are shown in Fig. 9. It can be seen that the isotherms cluster near the upper heat source is more substantial than the lower heat source for all values of Pe due to the difference in the value of the heat flux. Fig. 9(a) and (b) depict the isotherms of the buoyancy driven flows for $Pe = 1$ and $Pe = 10$, respectively, and these isotherms show positive slops. On the other hand, Fig. 9(e) and (f) show the forced convection domination with $Pe = 60$ and $Pe = 100$, respectively, and the isotherms show negative slopes. Further, Fig. 9(c) and (d), for $Pe = 20$ and $Pe = 40$, respectively, show the isotherms near the lower source with negative slopes and in contrast to that the isotherms near the upper source with positive slopes, which leads to increasing $\overline{Nu_1}$ and decreasing $\overline{Nu_2}$ with increasing Pe in this range as mentioned earlier and shown in Fig. 8.

5. Conclusions

The steady mixed convection flow adjacent to a vertical flat plate embedded in a fluid-saturated porous medium, on which two isolated thermal sources are located, is studied numerically using the Darcy law model. The non-dimensional governing equations are solved numerically using the finite volume method. The qualitative changes in the mixed aiding and mixed opposing flow patterns, when the two sources are located on the plate are very successfully captured in the present analysis. The governing parameters are the separation distance between the heated elements, their lengths and heat flux ratio in additional to the Rayleigh number, Péclet number and the external flow direction. The major results obtained can be summarized as follows. It is shown that in the cases where the buoyancy flow is dominant, the effect direction of the external flow is negligible. While the Rayleigh number has more substantial effect for buoyancy driven flow than that for external driven flows. For aiding flows, the values of the average Nusselt number along the lower heat source (leading source) are forming a single curve versus Pe for different values of D, L_2 or q_2/q_1, indicating independency of the heat transfer from the lower heat source. On the other hand, the heat transfer from the upper source is affected by the presence of the lower heat source. For aiding flow, it is found that the increase in any of the separation distance between the heated elements, their lengths or the heat flux ratio, leads to increase in the average Nusselt number along the upper heat source.

For opposing flow, when the external flow passing over the upper heat source first, the average Nusselt number along the two heat sources decreases with an increase in Pe to reach a minimum values before start increasing with Pe. Increasing Pe further, after the value, which gives the minimum values, the average Nusselt number along the lower heat source increases with the increase of the separation distance and it decreases with the increase in either the upper source length or the heat flux ratio. It has been shown also, for some combination of the governing parameters in the opposing flow case, that $\overline{Nu_1}$ can be increased with increasing Pe, in contrast to that, $\overline{Nu_2}$ is decreasing with increasing Pe due to the difference of the effective Rayleigh number near the two heat sources. Finally it should be mentioned that comparison with experimental data is beyond the scope of the present study due to lack of any experiments.

Acknowledgement

The authors wish to thank the anonymous referees for their valuable comments and suggestions.

References

[1] D.A. Nield, A. Bejan, Convection in Porous Media, second ed., Springer, New York, 1999.
[2] D.B. Ingham, I. Pop (Eds.), Transport Phenomena in Porous Media, Pergamon, Oxford, 1998 (vol. II, 2002).
[3] K. Vafai (Ed.), Handbook of Porous Media, Marcel Dekker, New York, 2000 (vol. II 2005).
[4] I. Pop, D.B. Ingham, Convective Heat Transfer: Mathematical and Computational Modelling of Viscous Fluids and Porous Media, Pergamon, Oxford, 2001.
[5] A. Bejan, A.D. Kraus (Eds.), Heat Transfer Handbook, Wiley, New York, 2003.
[6] D.B. Ingham, A. Bejan, E. Mamut, I. Pop (Eds.), Emerging Technologies and Techniques in Porous Media, Kluwer, Dordrecht, 2004.
[7] A. Bejan, I. Dincer, S. Lorente, A.F. Miguel, A.H. Reis, Porous and Complex Flow Structures in Modern Technologies, Springer, New York, 2004.
[8] H. Hadim, K. Vafai, Overview of current computational studies of heat transfer in porous media and their applications—forced convection and multiphase heat transfer, in: W.J. Minkowycz, E.M. Sparrow (Eds.), Advances in Numerical Heat Transfer, vol. II, Taylor and Francis, New York, 2000, pp. 291–329.
[9] K. Vafai, H. Hadim, Overview of current computational studies of heat transfer in porous media and their

applications—natural and mixed convection, in: W.J. Minkowycz, E.M. Sparrow (Eds.), Advances in Numerical Heat Transfer, vol. II, Taylor and Francis, New York, 2000, pp. 331–369.

[10] F.C. Lai, V. Prasad, F.A. Kulacki, Aiding and opposing mixed convection in a vertical porous layer with a finite wall heat source, Int. J. Heat Mass Transfer 31 (1988) 1049–1061.

[11] F.C. Lai, C.Y. Choi, F.A. Kulacki, Free and mixed convection in horizontal porous layers with multiple heat sources, J. Thermophys. 4 (1990) 221–227.

[12] F.C. Lai, F.A. Kulacki, V. Prasad, Mixed convection in saturated porous media, in: S. Kakaç, B. Kilkis, F.A. Kulacki, F. Arinç (Eds.), Convective Heat and Mass Transfer in Porous Media, Kluwer, Dordrecht, 1991, pp. 225–287.

[13] V. Prasad, F.C. Lai, F.A. Kulacki, Mixed convection in horizontal porous layers heated from below, Trans ASME J. Heat Transfer 110 (1988) 395–402.

[14] F.C. Lai, F.A. Kulacki, Oscillatory mixed convection in horizontal porous layers heated from below, Int. J. Heat Mass Transfer 34 (1991) 887–890.

[15] F.C. Lai, Mixed convection in saturated porous media, in: K. Vafai (Ed.), Handbook of Porous Media, Marcel Dekker, New York, 2000, pp. 605–661.

[16] Y. Jaluria, Mixed convection flow over localized multiple thermal sources on a vertical surface, Phys. Fluids 29 (1986) 934–940.

[17] S.V. Patankar, Numerical Heat Transfer and Fluid Flow, Hemisphere, Washington, DC, 1980.

[18] T. Hayase, J.A.C. Humphrey, R. Greif, A consistently formulated QUICK scheme for fast and stable convergence using finite-volume iterative calculation procedures, J. Comput. Phys. 98 (1992) 108–118.

[19] N.H. Saeid, Analysis of mixed convection in a vertical porous layer using non equilibrium model, Int. J. Heat Mass Transfer 47 (2004) 5619–5627.

[20] P. Cheng, Combined free and forced boundary layer flows about inclined surfaces in a porous medium, Int. J. Heat Mass Transfer 20 (1977) 807–814.

[21] J.C. Hsieh, T.S. Chen, B.F. Armaly, Mixed convection along a nonisothermal vertical flat plate embedded in a porous medium: the entire regime, Int. J. Heat Mass Transfer 36 (1993) 1819–1826.